polymer papers

The interpretation of electron microscope images and scattering patterns from crazes

H. R. Brown
Department of Macromolecular Science, Case Western Reserve University, Cleveland, Ohio 44106, USA
(Received 6 March 1984)

Images and small-angle diffraction patterns of crazes obtainable in the transmission electron microscope have been calculated from model structures using a single theory of interaction of electrons with the sample. The model was of a relatively thick craze so that many fibrils overlapped. The calculated defocused images of this model showed little obvious relationship to the original model showing that it is very hard to estimate craze fibril diameters from craze images. The calculated scattering pattern normal to the craze showed both the refraction and diffraction effects observed previously and so is in excellent accord with experiment.

(Keywords: crazes; electron microscope images; scattering patterns; fibrils)

INTRODUCTION

Crazes are planar, crack-like defects that form in most polymers in response to a tensile stress. They are distinct from cracks in that they are load bearing. The two craze surfaces are joined by material in a fine fibrillar morphology. Craze fibril diameters are typically in the range of 5–30 nm so the preferred technique for craze morphology studies has been transmission electron microscopy. Small-angle scattering has also been used a considerable amount recently with one of the radiations used being electrons. The majority of information available on craze microstructures has hence been obtained by TEM imaging and, to a lesser extent, small-angle electron scattering (SAES) in the TEM. Craze images obtained in this way are however not very easy to interpret. There are two main reasons for this: firstly, the images are of a system containing many overlapping fibrils, and secondly, the imaging process is a combination of scattering and phase contrast. These are also problems in the interpretation of craze SAES patterns; in particular in previous work the scattering normal to the craze has been divided rather arbitrarily into diffraction and refraction components.

Confidence in the interpretation of TEM diffraction patterns of images can be improved by a comparison of the experimental observations with results calculated from model structures using the transfer theory of imaging. That is the aim of the work described in this paper. This approach has previously been used in the synthetic polymer field by Thomas and coworkers[1,2] when considering electron microscope evidence for both order in glassy polymers and domain structures in urethanes.

THEORETICAL BACKGROUND

Transfer theory of imaging

The transfer theory of imaging is well described in a number of publications[3-5] and hence will not be repeated in detail here. The incident illumination can be considered as a planar coherent wave $\psi_0(x,y)$. The effect of the specimen is to alter the amplitude and phase of this wave to give an exit wave $\psi_e(x,y)$. The exit wave is then convoluted with a microscope transfer function $t(x,y)$ to give a bright field image $i(x,y)$ as

$$\psi_1(x,y) = t(x,y) \widehat{\psi}_e(x,y) \tag{1}$$

$$i(x,y) = \psi_1(x,y)\ \psi_1^*(x,y) \tag{2}$$

The process is easier to consider in Fourier Transform (scattering pattern) space where the transform is represented by the upper case symbol such that

$$\Psi(u,v) = \int \psi(x,y)\, e^{-2\pi i(ux+vy)} dx \cdot dy$$

The scattering pattern from the sample is given by $\Psi_e^*(u,v)\Psi_e(u,v)$.

The microscope transfer function is of the form

$$T(u,v) = A(u,v)e^{i\chi(u,v)} \tag{3}$$

where $A(u,v)$ is step function representing the objective aperture and χ is given by

$$\chi(u,v) = \pi\lambda(\Delta f)(u^2+v^2) + \pi/2 C_s\lambda^3(u^2+v^2)^2 \tag{4}$$

where C_s is the spherical aberration coefficient of the microscope and Δf the defocus. For the situations considered in this work, effects of the spherical aberration are insignificant and will not be considered further.

The image wave function is hence given by

$$\Psi_1(u,v) = T(u,v)\Psi_e(u,v) \tag{5}$$

so the image can easily be calculated as a function of defocus from the exit wave function.

0032-3861/85/040483-07$03.00

Interaction of the electron beam with the specimen

For a thin specimen, the interaction of the electron wave with the specimen can be described simply. The exit wave is the product of the incoming wave with the specimen transmission function $q(x,y)$.

$$\psi_e(x,y)=q(x,y)\psi_0(x,y) \tag{6}$$

The specimen changes both phase and amplitude of the wave. The phase change is controlled by the specimen refractive index, n, and path length l. The amplitude terms contain the decrease in beam intensity due to both inelastic scattering and high-angle elastic scattering, that is electrons that hit the objective aperture. Both phase and amplitude terms can be obtained either experimentally or theoretically[6,7]. The phase term has normally been derived theoretically from the relationship between refractive index and inner potential of a material[8]. A nonrelative approximation gives

$$q(x,y) = e^{-i\sigma\delta(x,y)}e^{-\mu(x,y)}$$

where $\delta(x,y)$ is the projection in the beam direction of the inner potential of the material so

$$\delta(x,y)=\int_0^l E(z)dz$$

and

$$\sigma=\frac{\pi}{\lambda V_0}$$

where λ is the electron wavelength and V_0 is accelerating voltage.

For situations such as crazes it is easier to work in terms of refractive index, n, and path length $l(x,y)$ within the specimen, in which case

$$q(x,y)=e^{-i\beta l(x,y)}e^{-\mu_0 l(x,y)} \tag{7}$$

where

$$\beta=\frac{2\pi(n-1)}{\lambda}$$

and μ_0 is the amplitude absorbtion coefficient for the material. The experimental determination of n will be considered later.

Cowley[7,8] and others have described theoretical approaches to obtain the absorbtion coefficient μ. This quantity can also be obtained experimentally from mass thickness contrast measurements[9,11] particularly for the material (polystyrene) considered in this work where varying size latex spheres are available and also uniform thin films are easy to make.

Normally thin polymer samples can also be considered as weakly scattering, that is to say, only the first term in the expansion of the exponential need be retained. Hence

$$q(x,y)\approx 1-i\sigma\delta(x,y)-\mu(x,y) \tag{8}$$

This approximation is valid in cases where the variations across the sample of the projected potential ϕ are relatively small. The mean value of ϕ is unimportant as it just adds a constant phase shift to the exit wave. For example Roche and Thomas have demonstrated the validity of this expression for film thickness up to 70 nm in polyethylene where the spacial fluctuations in potential come from the relatively small density differences between the crystalline and amorphous regions[2]. It is however not valid for even a single large craze fibril (diameter 20 nm) let alone a complete craze. This is because the potential difference between craze fibril and void is so large[11].

A thin sample is one in which the spread of the electron beam is insignificant compared with the resolution of interest. Cowley and Moodie have demonstrated that the spread can be well described by convoluting the wavefunction with the Fresnel diffraction formula

$$\psi_2(x,y)=\psi_1(x,y)\widehat{p}(x,y) \tag{9}$$

where $p(x,y)$ is the propagator given in small-angle scattering by[5]

$$p(x,y)=\left(\frac{i}{R\lambda}\right)\exp\frac{-ik(x^2+y^2)}{2R} \tag{10}$$

R is the distance of propagation between ψ_1 and ψ_2. An estimate of the spread can be obtained by considering the value of x for which $kx^2/2R=\pi$. For λ equal to 0.003 nm and R equal 400 nm (a typical specimen thickness for craze studies) then x is 1.1 nm. This spread is significant in comparison with fibril diameters which are in the range of 5–20 nm.

When the spread is significant then the thin specimen approximation can no longer be used. Cowley and Moodie have shown that a thick specimen can be considered as a series of slices where each slice can individually be considered as thin but the propagation term from slice to slice must be included[5]. The total specimen interaction is therefore considered as a series of transmission and propagation processes. This is the multi-slice formulation. For the n^{th} slice, the exit wave from the $(n-1)^{th}$ slice is $\psi_{n-1}(x,y)$ then

$$\psi_n(x,y)=[\psi_{n-1}(x,y)\widehat{p_\Delta}(x,y)]q_n(x,y) \tag{11}$$

where Δ is the distance between slices. The exit wave function from the specimen can hence be calculated by modification of the input wave function by a series of these convolution and multiplication operations. It is often convenient to work in terms of the Fourier transforms where the equivalent equation is:

$$\Psi_n(u,v)=[\Psi_{n-1}(u.v)\cdot P_\Delta(u,v)]\widehat{Q}_n(u,v) \tag{12}$$

This formulation is easy to program and hence convenient for the prediction of craze images. Results using this approach will be presented later.

MODELS

The work described in this paper is concerned with the calculation of both craze diffraction patterns and images using the theory described in the previous section. The diffraction (or scattering) pattern of a craze can be considered in two parts, as it is in the shape of a cross. One part is caused by diffraction from the craze fibrils and the other by the diffraction from the craze–matrix interfaces. Diffraction from the craze fibrils is sensitive to the local arrangement of these fibrils as described by their radial distribution function (r.d.f.). It would not be easy to set up a model with a plausible r.d.f., particularly as such a model would have to be fairly large. This was not attempted in this work, so only scattering normal to the craze–matrix

interface will be considered. For the prediction of scattering normal to the craze–matrix interface, the craze can be modelled as a slit containing material of lower density than the surroundings. The relative density within the slit is v_f, the volume fraction of fibrils within the craze. The results from this model will be presented later in this paper.

Calculation of craze images will be considered in two stages. First results will be given for single fibrils as a function of fibril size and defocus using the thin specimen approximation and then layers of these fibrils will be combined in a multi-slice calculation to predict images of whole crazes.

A single craze fibril of diameter D can be considered as a long cylinder with axis normal to the beam so only a one-dimensional calculation is necessary and

$$l(x)=D\left(1-\left(\frac{2x}{D}\right)^2\right)^{1/2} \tag{13}$$

In constructing a layer, a certain model size L was assumed and the number of fibrils given by $L/2D$. With the layers assumed to be a distance $2D$ apart this gave a fibril volume function v_f of 0.196 which is a reasonable value for polystyrene. Two different systems for distribution of the fibrils with the layers were used. In the first of these the fibrils were distributed randomly on the layer with no concern for fibril overlap. The second distribution was of a pseudo-lattice type where the fibril axis was placed at random within a distance $D/2$ from its lattice site so there was no overlap. Images calculated using these two models were indistinguishable.

CALCULATIONS AND RESULTS

Scattering normal to the craze–matrix interface

The scattering normal to the craze–matrix interface has two components, a simple diffraction component and a refraction component which is only significant when the specimen is tipped about an axis along the craze. This latter scattering has been described in an earlier publication where it was analysed using geometrical optics and used to measure the refractive index of polystyrene[6].

In this work the scattering will be considered as a function of specimen tip angle θ, craze width t and specimen thickness d. The geometry is shown in *Figure 1*. For convenience the phase and amplitude of the exit wave ψ_e are assumed to be 0 and 1 respectively away from the craze. As only low resolution is of relevance, the thin specimen approximation may be used and so

if $$f=\frac{t\mathrm{Cos}\theta-d\mathrm{Sin}\theta}{2} \tag{14}$$

$$g=d\mathrm{Sin}\theta$$

and $$\psi_e=e^{i\phi(x)\mu(x)} \tag{15}$$

for $|x|<f \quad \phi=\phi^* \quad \mu=\mu^*$

for

$$f\leqslant|x|<f+g \quad \phi=\phi^*\left(1-\frac{|x|-f}{g}\right):\ \mu=\mu^*\left(1-\frac{|x|-f}{g}\right):$$

for $f+g\leqslant|x| \quad \mu=\phi=0$

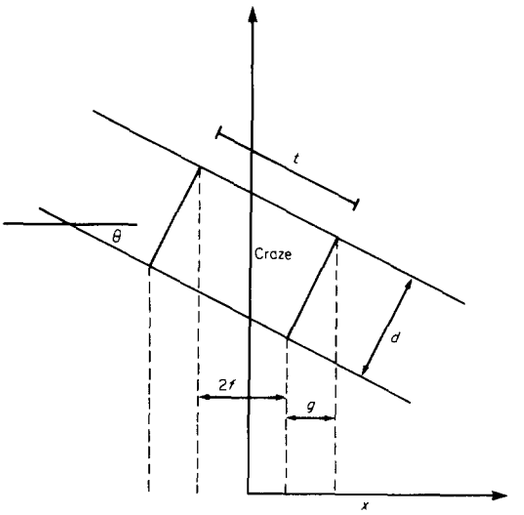

Figure 1 Geometry of a crazed film tipped by an angle θ about an axis along the craze

and $$\phi^*=\frac{d(n-1)(1-v_f)2\pi}{\lambda\mathrm{Cos}\theta} \tag{16a}$$

$$\mu^*=\frac{d(1-v_f)\mu_0}{\mathrm{Cos}\theta} \tag{16b}$$

The diffraction pattern, $\Psi(u)$ is given by a sum of terms

$$\Psi(u)=\Psi_1(u)+\Psi_2(u)+\Psi_3(u) \tag{17}$$

where

$$\Psi_1(u)=[1-e^{(i\phi^*+\mu^*)}]\frac{2\mathrm{Sin}uf2\pi}{2\pi u} \tag{18a}$$

$$\Psi_2(u)=\mathrm{Sin}\left(\frac{2\pi ug}{2}\right)\cos\left[2\pi u\left(\frac{f+g}{2}\right)\right]\frac{4i}{2\pi u} \tag{18b}$$

$$\Psi_3(u)=-e^{(i\phi^*+\mu^*)(1+f/g)}[(e^{\alpha(f+g)}-e^{\alpha f})/\alpha + (e^{-\beta(f+g)}-e^{-\beta g})/\beta \tag{18c}$$

where

$$\alpha=i(-\phi^*/g+2\pi u)^{-\mu^*}/g:\ \beta=i(\phi^*/g+2\pi u)+\mu^*/g \tag{18d}$$

The first and second terms (equations (18a) and (18b)) are the classic diffraction from the slit. The third term, equation (18c), is equivalent to the refraction term obtained previously by geometrical optics. This can be seen from the fact that it will have peaks when α and β are minima, or when

$$2\pi u=\pm\frac{\phi^*}{g} \tag{19}$$

The deflection angle η (given as $\Delta\phi$ in the previous work) is hence given by

$$u=\frac{\eta}{\lambda} \tag{20}$$

then from equations (14) and (16a)

$$\eta=(n_1-n_2)\left(\tan\theta+\tan\left(\frac{\pi}{2}-\theta\right)\right)$$

as before.

The diffraction pattern intensity $\Psi \cdot \Psi^*$ has been calculated from equation (17) for a series of specimen widths, craze widths and tip angles. Craze fibril volume fraction v_f was assumed to be 0.2, a typical value for polystyrene crazes. The value of 3.16×10^{-5} measured previously was used for $n-1$. The absorption coefficient, μ_0, was measured from microdensitometer scans across infocus images of latex spheres. The value used was 0.003 nm^{-1}, a fairly typical value for a small objective aperture in a 100 kV microscope. The results are given in *Figures 2–4*.

Figure 2 shows the effect of changing the specimen tip angle with film thickness and craze widths both held constant at 400 nm. This is a fairly typical value for both parameters. It can be seen from this figure that the primary effects of tipping the specimen are to alter the position, width and height of the 'refraction' peak. The peak becomes narrower and more intense at the higher angles. This result is entirely in accord with experimental observations[6,12]. *Figure 3* shows that with decreasing craze width, the relative height of the refraction peak increases though its width stays constant.

It is clear in the results shown in *Figure 4* that the intensity and sharpness of the refraction peak increase with specimen thickness. In addition, as would be expected from equation (18b), specimen thickness affects the forms of the inner diffraction maxima when the tip angle θ is significant.

All these results are in accord with experimental observations[12] and demonstrate that this approach to the calculation of the scattering pattern normal to the craze–matrix interface agrees very well with experiment. It has the great advantage of not requiring the arbitrary separation of the pattern into refraction and diffraction.

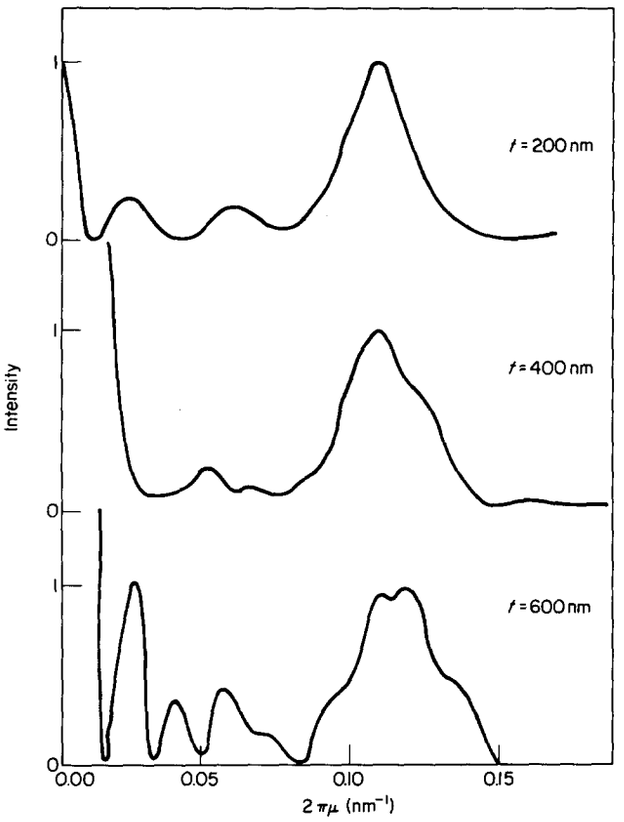

Figure 3 As for *Figure 2* for $\theta = 25°$ with craze width $t = 200$, 400 and 600 nm

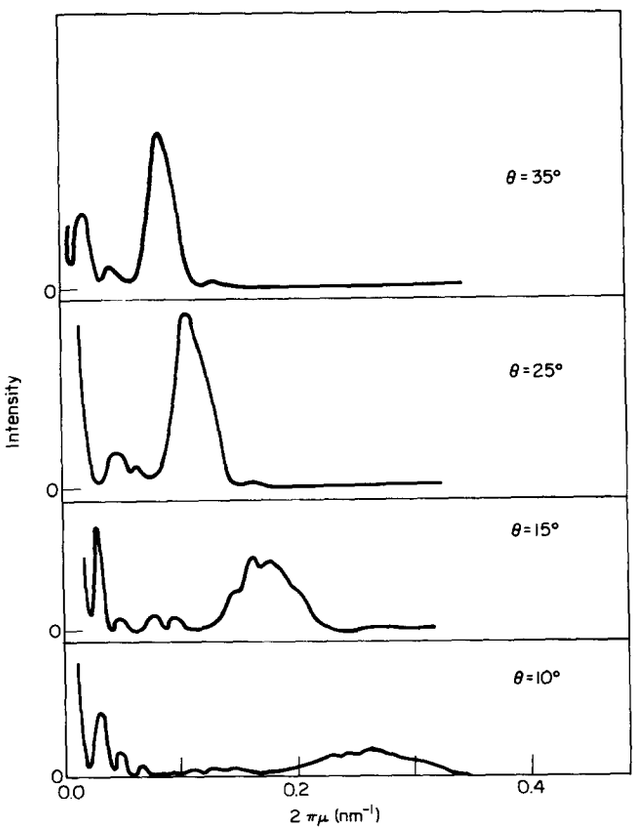

Figure 2 Scattering patterns normal to the craze as a function of tip angle θ with both craze width and film thickness equal to 400 nm and craze v_f equal to 0.2

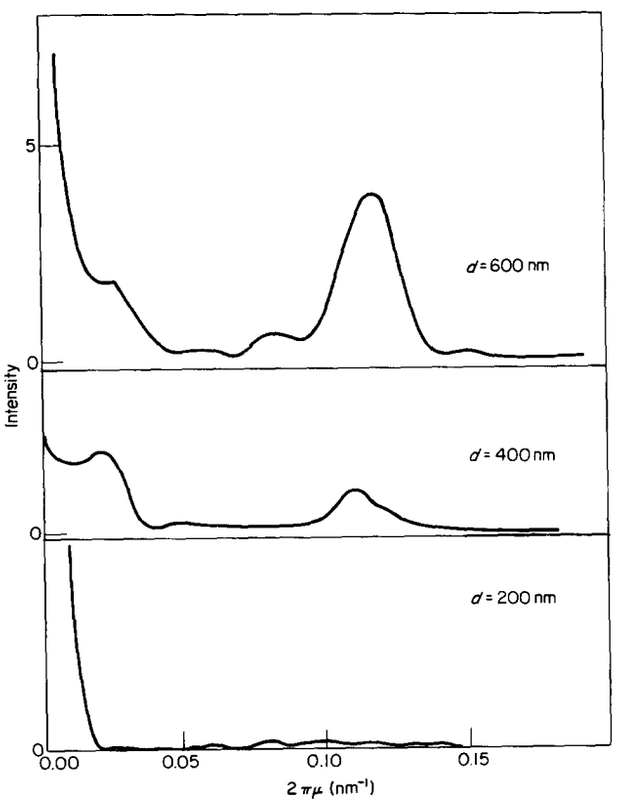

Figure 4 As for *Figure 2* for $\theta = 25°$ with film thickness $d = 200$, 400 and 600 nm

Images of single craze fibrils

Images of single fibrils were calculated using equations (5), (6), (7) and (13) as described earlier. Results are given in *Figures 5* and *6* for two fibril diameters, 10 and 20 nm, and defocus of 0, -1 μm and -3 μm. The same values of n and μ_0 were used as in the previous calculation.

These images show the large effects of defocus on the contrast. This is typical in TEM of relatively transparent objects; very similar results for both lamella structures[2] and cylinders[8] have been published previously.

These results demonstrate that even with a small objective aperture the contrast from a single craze fibril is relatively low but can be very considerably increased by using a large amount of defocus. The relatively small change in contrast obtained by doubling the fibril diameter demonstrates that for an image of separated fibrils of various sizes, there is little bias in the sense that either big or small fibrils will be observed preferentially.

Craze images are however not normally made up of separated fibrils. Only a few materials craze in films thin enough to give separated fibrils and in one of them, polystyrene, it is well demonstrated that these crazes are different in structure from those in thicker films[13]. To understand crazes in thicker films, it is necessary therefore to calculate images of many overlapping fibrils. That will be considered in the next section.

Images of crazes consisting of many overlapping fibrils

The multi-slice technique described earlier was used to calculate the images from a number of overlapping layers of fibrils. The fibrils were assumed to have a diameter of 5 nm and so the layers were 10 nm apart. Up to 20 layers, a specimen thickness of 200 nm, were used and images were calculated as a function of defocus, number of layers and random number seed. The total model size L was 60 nm. The effect of specimen thickness on the results was

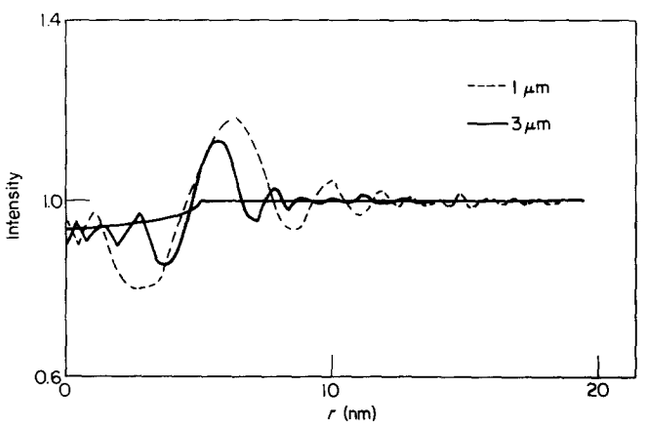

Figure 5 Calculated image of a single fibril of diameter 10 nm and defocus of 0, -1, and -3 μm

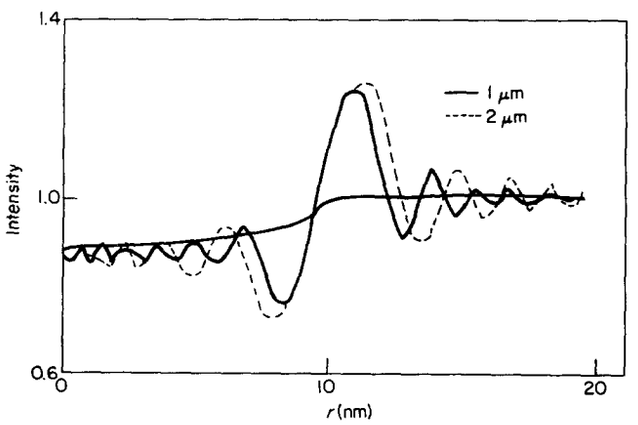

Figure 6 Calculated image of a single fibril of diameter 20 nm and defocus of 0, -1 and -3 μm

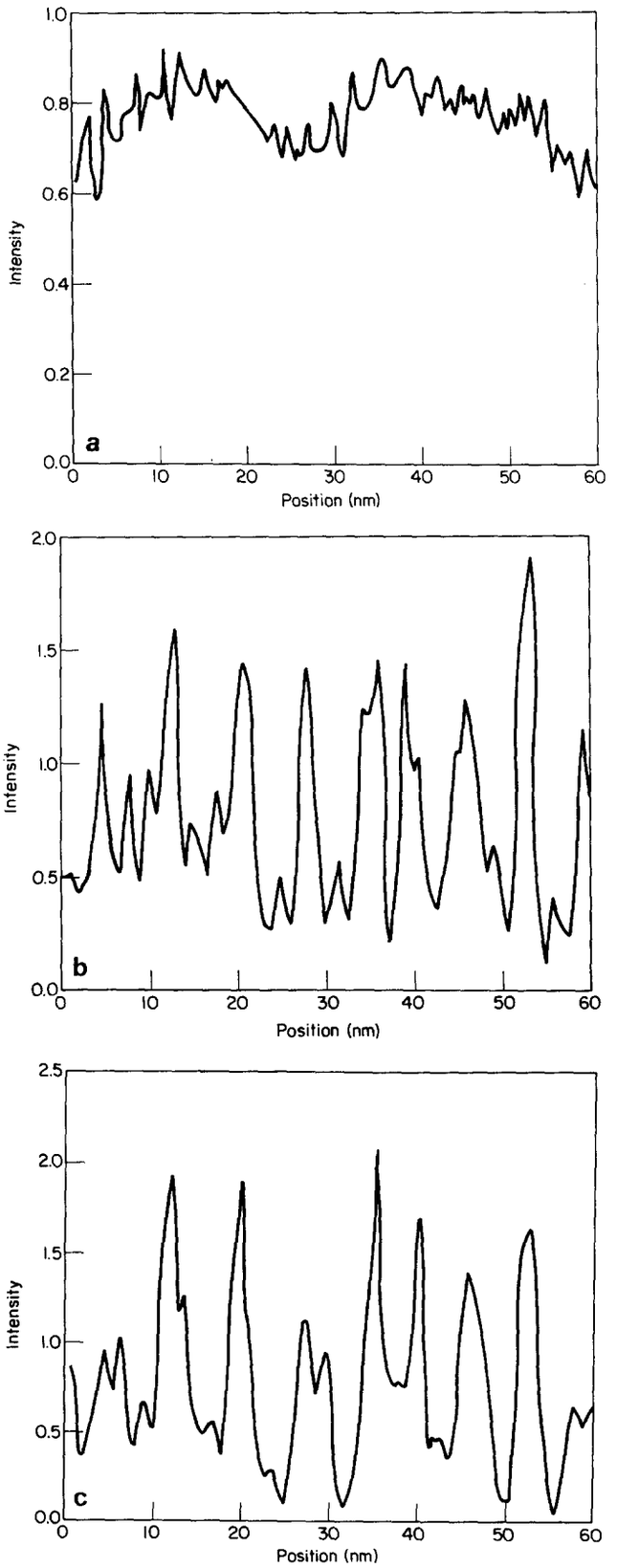

Figure 7 Calculated craze image with defocus equal to 0 (*Figure 7a*), -3 μm (*Figure 7b*), and -5 μm (*Figure 7c*)

examined by doing some calculations with the propagators set equal to 1. This is equivalent to going to the thin specimen approximation.

Figure 7 shows in focus and $-1\ \mu m$, $-3\ \mu m$ and $-5\ \mu m$ defocus images of a 20 layer model. The effect is very large; there is very little contrast in the infocus image and the contrast increases massively on defocus. The reason for this small contrast in focus can be seen by comparing *Figure 7* with *Figure 8* in which the propagators have been set equal to 1. Clearly the defocus effects caused by specimen thickness remove the detail from the in focus image. The defocused equivalent of *Figure 8* is not shown, as it was indistinguishable from that in *Figure 7*. The effects of specimen thickness become entirely insignificant when the microscope is operated at a considerable defocus.

An interesting feature of the images of *Figure 8* is that there would be no way to tell them that they are images of a structure consisting entirely of 5 nm diameter fibrils. In fact, from the defocused image one might be more tempted to guess that the structure consisted of a range of fibril sizes of 6 to 10 nm. These results demonstrate very clearly the impossibility of estimating craze fibril sizes from a naive interpretation of TEM images. The effects of specimen thickness, shown by comparison of *Figures 7* and *8*, also show that optical diffraction patterns taken from in focus images will give very little information.

Figure 7 is just one image using a particular set of random numbers and it is necessary to check that it is typical. *Figures 9* and *10* are entirely equivalent except for the use of different random number seeds. They are essentially similar to *Figure 7*.

The effects of defocus shown in *Figure 7* are entirely in accord with experimental observations. Craze images show very little contrast when in focus. As they are underfocused, initially the contrast increases rapidly but after a while when there is 'sufficient' defocus, the focus makes very little difference.

DISCUSSION AND CONCLUSIONS

The results described in this work all use a single model for both the interaction of the electron beam with the specimen and the imaging process within the TEM. The same material parameters, n and μ_0, were used throughout. Hence they provide a unified picture of electron scattering patterns and images of crazes. That picture agrees well with experimental observations. Unfortunately due to computing limitations, it was not practical to construct a model large enough to calculate reasonable fibril diffraction patterns. That will be done in the future.

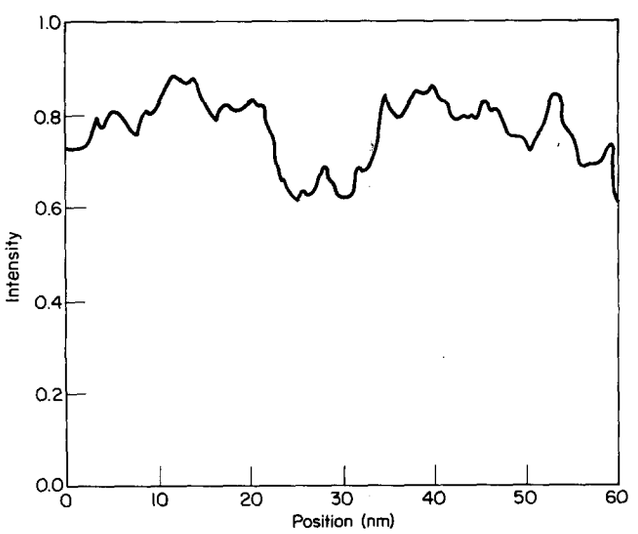

Figure 8 Calculated zero defocus image of the same craze as shown in *Figure 7* but propagators set to zero

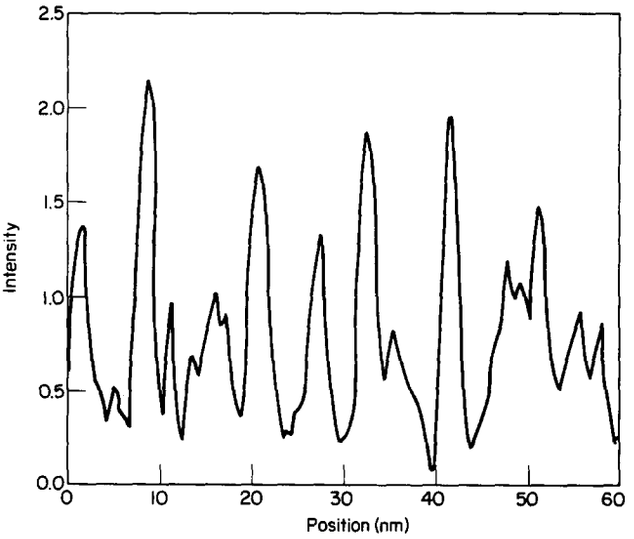

Figure 9 A similar image to *Figure 7b* but with a different random number seed

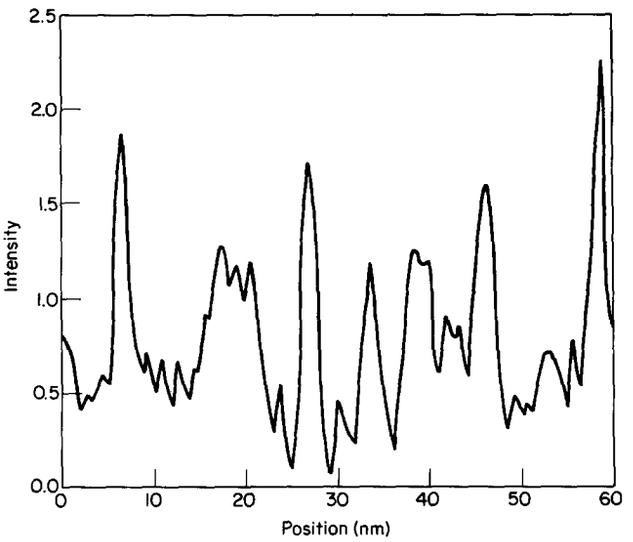

Figure 10 Similar to *Figure 9*

The main conclusions to be obtained from this work are that the propagation effects within thick specimens remove detail from the infocus image and make analysis impossible. Defocused pictures, though containing much contrast and detail are very hard to interpret and so it is not possible to obtain reliable information on craze structures from either infocus or defocused images of thick films. It is not yet evident if the interpretation of small-angle electron scattering patterns from the fibrils will be any clearer, as the specimen thickness increases the spacial fluctuations in phase shift become significant with respect to π and the Rayleigh–Gans theory starts to break down. It seems likely that the diffraction pattern width will increase and so a Rayleigh–Gans based interpretation[11] would tend to underestimate the fibril size.

It appears therefore that the TEM is not suitable for

obtaining quantitative information on fibril sizes and size distributions in thick crazes.

ACKNOWLEDGEMENT

The author wishes to acknowledge the support of the National Science Foundation and Materials Research Laboratory at Case Western Reserve University under Grant No. DMR81-19425.

REFERENCES

1 Thomas, E. L. and Roche, E. J. *Polymer* 1979, **20**, 1413
2 Roche, E. J. and Thomas, E. L. *Polymer* 1981, **22**, 333
3 Hanszen, K. 'Advances in Optical and Electron Microscopy, 4', (Eds. R. Barer and V. E. Cosslett), Academic Press, London, 1971
4 Erickson, H. P. 'Advances in Optical and Electron Microscopy, 5', (Eds. R. Barer and V. E. Cosslett), Academic Press, London, 1973
5 Cowley, J. M. 'Diffraction Physics', North Holland, Amsterdam, 1975
6 Brown, H. R. *Ultramicroscopy* 1982, **7**, 263
7 Cowley, J. M. 'Introduction to Analytical Electron Microscopy', (Eds. J. J. Hren, J. I. Goldstein and D. C. Joy), Plenum, New York, 1979
8 Crintron, G. R. and Cowley, J. M. *Optik* 1971, **34**, 221
9 Brown, H. R. *J. Mater. Sci.* 1979, **14**, 237
10 Lauterwasser, B. D. and Kramer, E. J. *Phil. Mag.* 1979, **39A**, 469
11 Brown, H. R. *J. Polym. Sci. Polym. Phys. Edn.* 1983, **21**, 483
12 Sindoni, Y., unpublished work
13 Donald, A. M., Chan, T. and Kramer, E. J. *J. Mater. Sci.* 1981, **16**, 669